Journal of Medicinal Chemistry Article

J. Med. Chem. **2010,** *53,* 7119–7128 **7119**
DOI: 10.1021/jm100754z

Click-Chemistry-Derived Triazole Ligands of Arginine−Glycine−Aspartate (RGD) Integrins with a Broad Capacity To Inhibit Adhesion of Melanoma Cells and Both in Vitro and in Vivo Angiogenesis

Andrea Trabocchi,[†,‡] Gloria Menchi,[†,‡] Nicoletta Cini,[†,‡,§,∥] Francesca Bianchini,[‡,⊥,∥] Silvia Raspanti,[‡,§,∥] Anna Bottoncetti,[‡,§,∥] Alberto Pupi,[‡,§,∥] Lido Calorini,*[,‡,⊥,∥] and Antonio Guarna*[,†,‡]

[†]*Department of Chemistry "Ugo Schiff", University of Florence, Via della Lastruccia 13, 50019 Sesto Fiorentino, Florence, Italy,* [‡]*Interdepartmental Center for Preclinical Development of Molecular Imaging (CISPIM), University of Florence, Viale Morgagni 85, 50134 Florence, Italy,* [§]*Department of Clinical Physiopathology, Nuclear Medicine Unit, University of Florence, Italy,* [∥]*Istituto Toscano Tumori, Via T. Alderotti 26N, 50139 Florence, Italy, and* [⊥]*Department of Experimental Pathology and Oncology, University of Florence, Viale Morgagni 50, 50134 Florence, Italy*

Received June 21, 2010

A click chemistry approach was applied for the discovery of triazole-based arginine−glycine−aspartate (RGD) mimetics by Cu(I)-catalyzed 1,3-dipolar alkyne−azide coupling reaction, which showed binding affinity properties toward $\alpha_v\beta_3/\alpha_v\beta_5$ integrins. Biological assays showed compound **18** capable of binding $\alpha_v\beta_3$ integrin with nanomolar affinity according to a two-sites model, and molecular modeling studies revealed a peculiar π-stacking interaction between the triazole ring and Tyr178 side chain. Accordingly, compound **18** inhibited the adhesion of integrin-expressing human melanoma cells to RGD-containing proteins of the extracellular matrix, such as vitronectin, fibronectin, and osteopontin, and also angiogenesis in in vitro and in vivo experimental models. The relevant biological effects exerted by compound **18** suggest its potential application as an antiangiogenic agent in the diagnosis and therapy of tumors where $\alpha_v\beta_3$ integrin expression is up-regulated.

Introduction

Integrin receptors constitute a large family of proteins with structural characteristics of noncovalent heterodimeric glycoproteins formed of α and β subunits.[1] One important recognition site for many integrins is the arginine−glycine−aspartic acid (RGD[a]) tripeptide sequence,[2] found in a series of peptide-based ligands such as vitronectin, fibronectin, and osteopontin. Regarding RGD-dependent integrins, $\alpha_v\beta_3$ and $\alpha_v\beta_5$ receptors have received increasing attention as therapeutic targets, as they are expressed in various cell types and are involved in inflammatory and tumor-related processes.[3] $\alpha_v\beta_3$ integrin expression is up-regulated in many solid tumors and contribute to the mechanisms involved in tumor growth and metastatic dissemination.[4,5] During the progression from a benign melanocytic disease to a metastatic malignant melanoma, melanocytes undergo a series of changes in the expression of cell-surface molecules, including $\alpha_v\beta_3$ integrin.[6] In particular, an enhanced expression of $\alpha_v\beta_3$ integrin in melanocytes correlates with the invasive phase of human melanoma, namely, the vertical growth phase (VGP).[7] $\alpha_v\beta_3$ integrin was found to be localized at the invasive front of melanoma, where it may regulate the activity of matrix-degrading proteases, such as matrix metalloproteases and urokinase-type plasminogen activator, and cell motility.[8] Moreover, $\alpha_v\beta_3$ integrin is not only involved in tumor cell movement but also is essential in the regulation of endothelial cell growth and differentiation, and angiogenesis is crucial for tumor growth and dissemination. An important finding demonstrated that, unlike quiescent endothelium, endothelial cells of tumor vasculature express a high level of $\alpha_v\beta_3$ integrin. Thus, the involvement of $\alpha_v\beta_3$ integrin in tumor cell invasion and angiogenesis has inspired scientists to search RGD mimetics to be used for targeting growth and dissemination of cancer cells as well as to inhibit tumor neoangiogenesis.[9] The RGD recognition site can be mimicked by linear and cyclic peptides, and their specificity can be modulated by the sequence and structure of such peptides. $\alpha_v\beta_3$ antagonists, including RGD-containing peptides, have been successfully applied as inhibitors of blood vessel development and tumor growth.[10] Moreover, non-peptide RGD peptidomimetics have been developed as integrin ligands.[11]

Fragment-based assembly is a recently developed drug discovery approach that enables high-throughput identification of small molecule inhibitors using a minimal number of compounds as building blocks.[12] The approach is powerful especially against protein targets that possess multiple binding pockets in their active sites. Among different methods proposed to assist the assembly of compounds, "click chemistry", pioneered by Sharpless et al.,[13] is highly versatile, and it has become

*To whom correspondence should be addressed. For L.C.: +39 055 4598207; fax, +39 055 4598900; e-mail, lido.calorini@unifi.it. For A.G.: phone, +39 055 4573481; fax, +39 055 4573569; e-mail, antonio.guarna@unifi.it.

[a] Abbreviations: RGD, Arg-Gly-Asp; VGP, vertical growth phase; HIV, human immunodeficiency virus; SARS, severe acute respiratory syndrome; SEM, standard error of the mean; compd, compound; MIDAS, metal-ion dependent adhesion site; PDB, Protein Data Bank; RT-PCR, real time protein chain reaction; OPN, osteopontin; VN, vitronectin; FN, fibronectin; HUVEC, human umbilical vein endothelial cells; IL-1β, interleukin-1β; bFGF, basic fibroblast growth factor; ESI-MSMS, electropray ionization tandem mass spectrometry; EGM-2, endothelial cell growth medium-2; EDTA, ethylenediaminetetraacetic acid; GAPDH, glyceraldehyde 3-phosphate dehydrogenase; FACS, fluorescence-activated cell sorting; FITC, fluorescein isothiocyanate; PBS, Phosphate buffered saline.

Published on Web 09/01/2010

Chart 1. Selected Azides and Alkynes for the Click Chemistry Reaction

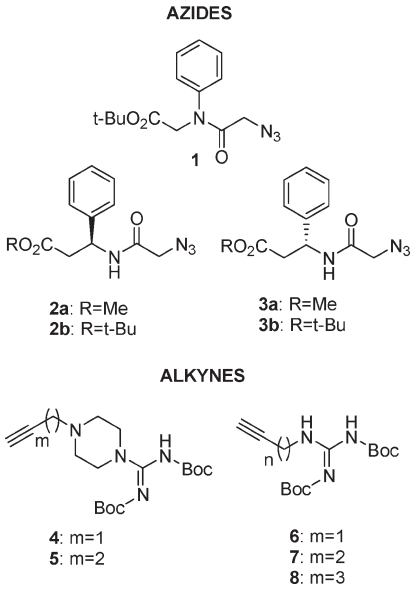

increasingly popular for generating new chemical entities in medicinal chemistry, in bioconjugating strategies, and in material chemistry. The mild and regioselective features of the Cu-catalyzed Huisgen 1,3-dipolar cycloaddition are particularly suited for developing combinatorial libraries containing the triazole ring, which has been applied successfully as amide bond isostere in peptidomimetic approaches. For example, it has been used in several drug discovery issues, including the generation of inhibitors against HIV protease, SARS 3CL protease, *R*-fucosidase, sulfotransferase, and *R*-1,3-fucosyltransferase.[14]

We envisaged using this strategy for generating RGD mimetics by virtue of combining azides and alkynes bearing Asp and Arg isosteres, respectively. Accordingly, the triazole ring was conceived as the Gly mimetic, thus acting as a spacer. Specifically, based on the reference integrin ligand cilengitide, azides containing a carboxylic group and an aromatic ring were taken into account as mimetics of both Asp and D-Phe pharmacophoric moieties, whereas alkynes differing in length and molecular shape were conceived as Arg mimetics (Chart 1).

Results

Synthesis. Triazole-based RGD ligands were achieved using click chemistry and specifically by combining azides **1**−**3** and alkynes **4**−**8** (Chart 1) in the Cu-catalyzed azide−alkyne cycloaddition, followed by acid-mediated hydrolysis of the protecting groups of side chain isosteres (see Scheme 1 for a representative synthesis).

Interestingly, the Cu-catalyzed reaction with these components proved to proceed in poor yields when the metal was used in catalytic amounts. Thus, a full equivalent of the copper salt was used, and longer reaction times were necessary to drive the reaction to completion, compared to standard conditions usually employed for reported applications of the click chemistry. This effect could be possibly due to the azide component, which inactivated the Cu catalyst by virtue of complexation reactions. The process allowed the rapid preparation of a library of triazole-containing RGD mimetics in 43−68% yields, as shown in Chart 2.

Receptor Binding Assays. The ability of triazole-containing RGD peptidomimetics to compete with [^{125}I]echistatin

Scheme 1. Representative Synthesis of Triazole-Based RGD Peptidomimetics: Preparation of Compound **18**

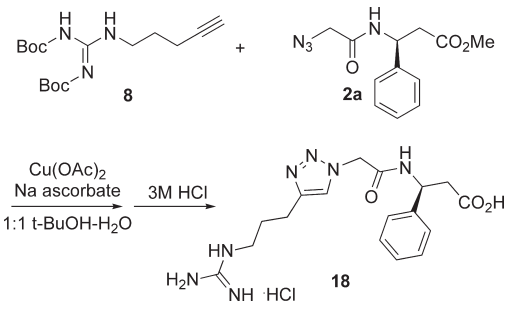

Chart 2. Panel of Triazole-Containing RGD Peptidomimetics

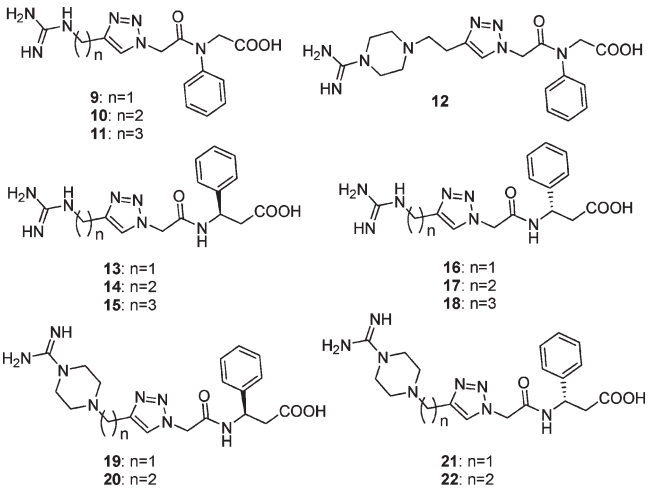

for binding to isolated, purified $\alpha_v\beta_3$ and $\alpha_v\beta_5$ integrins originated from human placenta[15] was evaluated in solid-phase receptor assays.[16] Competition studies were carried out using a fixed concentration of the radioligand (0.05 and 0.1 nM for $\alpha_v\beta_3$ and $\alpha_v\beta_5$ receptors, respectively) and a range of concentrations (100 μM to 0.01 nM) of the tested molecules. The $IC_{50} \pm$ SEM values (nM) were calculated as the concentration of compound required for 50% inhibition of radioligand binding, as estimated by the GraphPad Prism program, and the results are reported in Table 1.

IC_{50} values showed a binding affinity in the micromolar range for compounds **17**, **18**, and **20** toward $\alpha_v\beta_3$ and $\alpha_v\beta_5$

Table 1. Inhibition of [^{125}I]Echistatin Specific Binding to Purified Human Integrin Proteins $\alpha_V\beta_3$ and $\alpha_V\beta_5$ by Triazole-Containing RGD Peptidomimetics

	$\alpha_v\beta_3$		$\alpha_v\beta_5$	
compd	IC_{50} (μM)	Hill	IC_{50} (μM)	Hill
9	>10		>10	
10	>10		>10	
11	>10		>10	
12	>10		>10	
13	>10		>10	
14	>10		>10	
15	>10		46.3 ± 9.7	−0.899
16	>10		1.78 ± 0.30	−0.806
17	3.47 ± 0.76	−0.567	4.38 ± 0.51	−0.919
18	1.35 ± 0.25	−0.381	1.02 ± 0.12	−0.798
19	>10		>10	
20	4.96 ± 0.83	−0.877	2.42 ± 0.3	−1.037
21	>10		>10	
22	>10		1.27 ± 0.18	−0.810

Table 2. Inhibition of [^{125}I]Echistatin Specific Binding to Purified Human Integrin Proteins $\alpha_v\beta_3$ and $\alpha_v\beta_5$ by Selected Triazole-Containing RGD Peptidomimetics According to a Two-Sites Model

compd	$IC_{50,1}$ (nM)	$\%_1$	$IC_{50,2}$ (μM)	$\%_2$
		$\alpha_v\beta_3$		
17	1070 ± 210	55	70.7 ± 41	45
18	16.4 ± 2.0	35	3.42 ± 0.21	65
		$\alpha_v\beta_5$		
18	0.405 ± 0.27	59	4.24 ± 4.8	41

integrins, whereas compounds **15**, **16**, and **22** showed a more adaptive behavior only for $\alpha_v\beta_5$. Compounds **9**−**12** did not exhibit any binding affinity toward $\alpha_v\beta_3$ and $\alpha_v\beta_5$ integrins, suggesting the *N*-aryl moiety to impair the potency of triazole-containing RGD ligands. The configuration of the unique stereocenter proved to be crucial, as compound **18** showed the best binding affinity toward $\alpha_v\beta_3$, whereas the corresponsing enantiomer, i.e., compound **15**, did not show any activity toward such integrin. Such configurational specificity was reversed when the Arg isostere was changed to a guanidinylpiperazino derivative, as shown by binding affinities of compounds **20**−**22**. Also, homologated compounds **16**−**18** demonstrated a relationship between the binding affinity and the distance between Arg and Asp isosteres, thus allowing for the selection of **18** as the optimal ligand. The $\alpha_v\beta_3$ inhibition curves of active compounds showed Hill slope values different from unity, indicating the binding curve to be better described by a two-sites model, as a consequence of binding of the peptidomimetic compound with two conformational states of integrins, in agreement with other ligands already reported in the literature.[17] Thus, the analysis of the data with a nonlinear fitting indicated that these ligands bind to $\alpha_v\beta_3$ receptor according to a two-sites binding model (Table 2, Figure 1). It is possible that this effect could be due to a different affinity for the conformational states assumed by the integrins.[18] The transition from low- (bent form) to high-affinity (extended form) conformation has been described to be induced by natural ligands,[19] and also by most ligand-mimetic antagonists.[20] It was reported that some antagonists, such as the disintegrin echistatin, bind to the active and inactive forms with similar affinity, whereas others bind to the active form with higher affinity than to the inactive form.[21] Our results indicated compound **18** as a better ligand for $\alpha_v\beta_3$ integrin and to possess a selectivity by 2 orders of magnitude for $\alpha_v\beta_3$ with respect to $\alpha_v\beta_5$.

Molecular Modeling. A docking simulation using compound **18** and the available crystallographic data of $\alpha_v\beta_3$ integrin gave further insight into the possible binding modes of the selected ligand to $\alpha_v\beta_3$ at the molecular level. The crystal structure of the complex formed by *c*[RGDf(Me)V] (cilengitide) and the extracellular fragment of $\alpha_v\beta_3$ (PDB code 1L5G) provides a general mode of interaction between the integrin and its ligands.[20] The Asp carboxylate and Arg guanidinium moieties of RGD-based ligands are the two key structural elements for the receptor recognition. In fact, the carboxylate group interacts with the metal-ion-dependent adhesion site (MIDAS) consisting of Mn^{2+} ions and Ser121/Ser123, whereas the Arg guanidinium group is responsible for salt bridge interactions with the side chains of Asp218 and Asp150. Also, additional ligand−receptor contacts engage Tyr122 in hydrophobic π-stacking interactions and engage Asn215 and Arg216 in hydrogen-bonding contacts. The docking program Autodock 4.0.1[22] was used to evaluate the binding energies of the global minimum conformer of **18** as a ligand for $\alpha_v\beta_3$, and docked conformations were analyzed by taking into account the

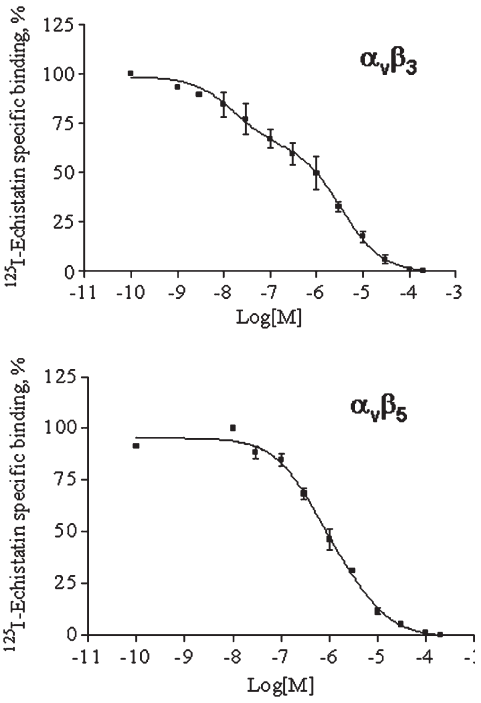

Figure 1. Inhibition curves of compound **18** toward $\alpha_v\beta_3$ and $\alpha_v\beta_5$ integrins.

binding interactions observed in the crystal structure of the ligand−protein complex. Docking results of compound **18** showed a main cluster of conformations displaying the typical binding mode of RGD cyclopeptide-based ligands (Figure 2, top, structures in green and yellow). Specifically, the main cluster showed the canonical binding mode consisting of Asp218/Asp150/guanidine and MIDAS/Ser121/carboxylate interactions. Interestingly, peptidomimetic **18** showed a somewhat different accommodation in the site, as the guanidinium group of the Arg side chain isostere experienced a monodentate interaction with both Asp218 and Asp150 instead of a bidentate interaction with Asp218. Moreover, a characteristic π-stacking interaction between the triazole ring and Tyr178 aromatic side chain was found in all the conformations of the main cluster, thus accounting for an additional stabilization of the ligand−receptor interaction (Figure 2, top). The analysis of the main cluster of docked conformations revealed a possible equilibrium between two conformers characterized by a π-stacking interaction between the aromatic ring of **18** and Tyr122 side chain (yellow structure, Figure 2, top right) and by a hydrogen bond between the Arg216 carbonyl group and the amide bond of **18** (green structure, Figure 2, top left), respectively.

A comparison of minimum energy conformations of **18** with the binding mode of the cyclopentapeptide reference ligand, *c*[RGDf(Me)V] (Figure 2, bottom, cyan structure), suggested a similar arrangement in the receptor's cavity, though displaying different secondary interactions. Specifically, the global minimum conformer of compound **18** (green structure) showed a hydrogen-bonding interaction with the Arg216 carbonyl group and a good superimposition of carboxylate and guanidino groups to Asp and Arg side chains of *c*[RGDf(Me)V] (Figure 2, bottom left), though not mimicking the hydrophobic π-stacking between D-Phe and Tyr122 aromatic side chains (Figure 2, bottom). On the contrary, the second low-energy conformation of compound **18** (Figure 2, bottom right, yellow structure), though displaying a worse

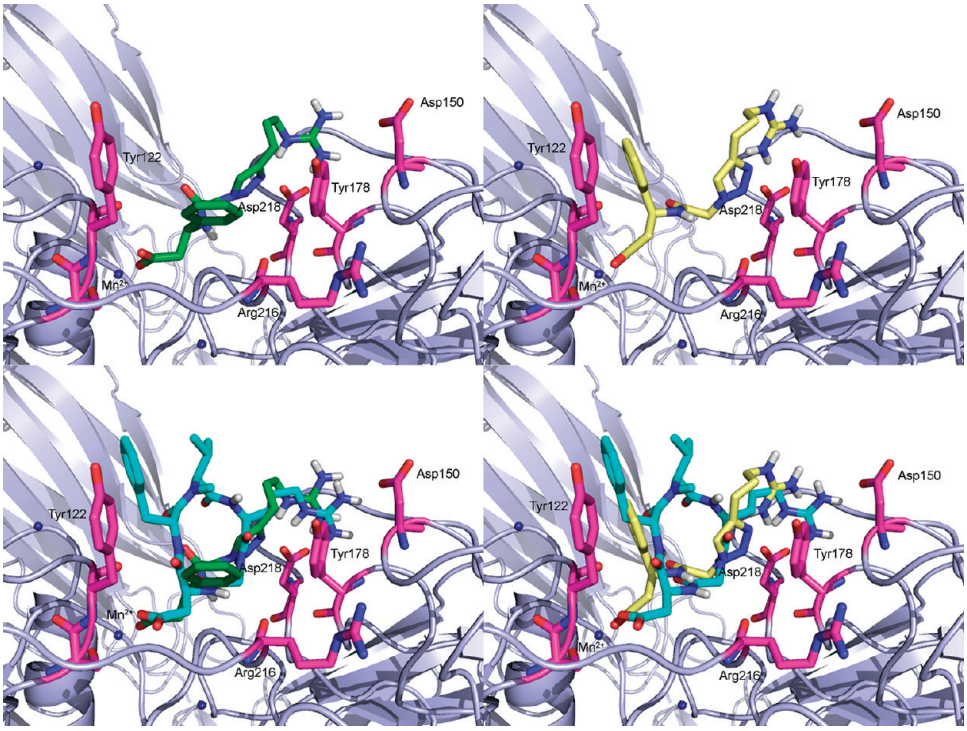

Figure 2. Top: Compound **18** (green to the left, yellow to the right) docked into the binding region of $\alpha_v\beta_3$, highlighting the protein residues (magenta) that form the key interactions. Bottom: Overlap between the reference ligand *c*[RGDf(Me)V] (cyan) and compound **18** (green to the left, yellow to the right) in the binding region of $\alpha_v\beta_3$ integrin. Nonpolar hydrogen atoms are omitted for clarity.

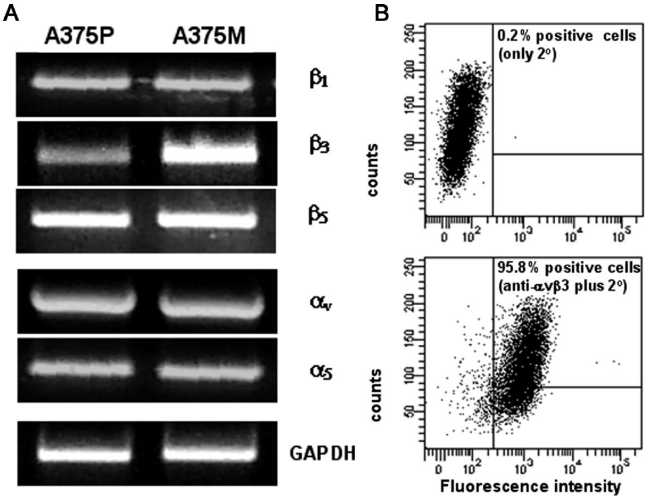

Figure 3. Integrin expression in human melanoma cells: RT-PCR analysis of integrin subunits in A375P and A375M melanoma cells (A); flow cytometry determination of $\alpha_v\beta_3$-positive cells in A375M line (B).

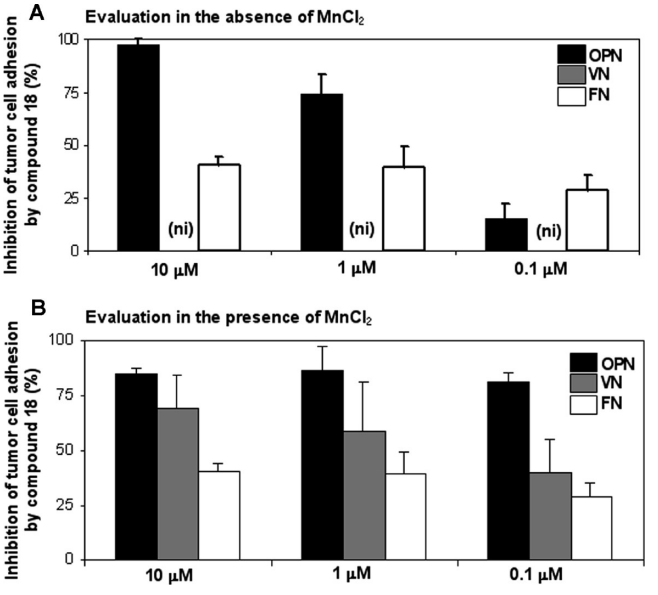

Figure 4. Inhibition values (%) of integrin-mediated A375M cell adhesion to osteopontin (OPN), vitronectin (VN), and fibronectin (FN) induced by compound **18**, tested in the absence (A) and in the presence (B) of Mn^{2+}. ni = no inhibition detected.

arrangement of pharmacophoric Asp and Arg isosteres, showed the π-stacking interaction with Tyr 122 side chain in analogy with the reference cyclopeptide (cyan).

Cell Biology Assays. Inhibition of Tumor Cell Adhesion to Proteins of the Extracellular Matrix. A series of experiments carried out using semiquantitative RT-PCR analysis allowed us to demonstrate that A375M human melanoma cells, a high lung metastatic variant of A375P cells isolated in hard agarose,[23] express a wide variety of integrin subunits (αV, β3, β5, α5, β1) (Figure 3A) and a high level of $\alpha_v\beta_3$ heterodimer, (Figure 3B). A375M melanoma line may well represent a suitable model of malignant cells to investigate the effects of RGD mimetics. A375M cells have been used to test the inhibitory capacity of compound **18**, used at 10, 1.0, and 0.1 μM, for tumor cell binding to important RGD-containing substrates such as vitronectin, fibronectin, and osteopontin.

Considering that the capacity of the cells to adhere to different substrates might be dependent on the ligand-binding affinity related to either the bent or the extended form of integrins, we tested the effects of compound **18** on the adhesion of tumor cells to RGD-containing substrates in the presence (Figure 4A) or in the absence of Mn^{2+} (Figure 4B). Mn^{2+} activates integrins

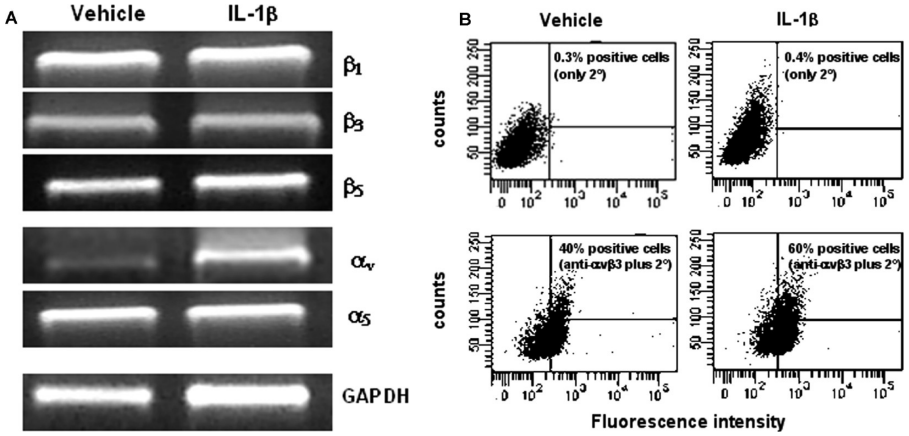

Figure 5. Integrin expression in HUVEC: RT-PCR analysis of integrin subunits in HUVEC and IL-1β-stimulated HUVEC (A); flow cytometry determination of $\alpha_v\beta_3$-positive cells in HUVEC and IL-1β-stimulated HUVEC (B).

directly by interacting with cation coordination sites in the βA domain, thus switching integrins from the bent form that binds ligands with low affinity to the extended form that binds ligands and carrying out outside-in signaling.[24] The results clearly showed that compound **18**, in the presence of Mn^{2+}, significantly inhibited the binding of melanoma cells to both vitronectin (with a dose-dependent effect) and osteopontin (even at nanomolar concentration), whereas it displayed an incomplete inhibition toward the adhesion of the cells to fibronectin. These results suggested that compound **18** displays a high affinity for $\alpha_v\beta_3$ and $\alpha_v\beta_5$ integrins and recognizes the RGD sequence exposed by vitronectin and osteopontin. Moreover, the findings that compound **18**, in the absence of Mn^{2+}, inhibited the binding of melanoma cells to osteopontin, although at a concentration of the product of 10 and 1 μM, and displayed no effect on the adhesion of tumor cells on vitronectin indicated that compound **18** displays a particular affinity for the activated form of $\alpha_v\beta_3$. The fact that the capacity of compound **18** to inhibit the adhesion of tumor cells on fibronectin was not modified by Mn^{2+} (inhibition in the region of 30−40%) revealed that the affinity of compound **18** is independent of the conformation of the receptor.

Inhibition of HUVEC Adhesion. RT-PCR (Figure 5A) and FACS analyses (Figure 5B) of the HUVEC (human umbilical vein endothelial cells) grown in the presence or in the absence of IL-1β indicate that these cells express integrin subunits (α_v, β_3, β_5, α_5, β_1) and $\alpha_v\beta_3$ heterodimer, mainly after IL-1β stimulation. IL-1β stimulated HUVEC mimic the activated endothelial cells found in tumor angiogenesis.

Before the evaluation of the potential antiangiogenic capacity of compound **18**, we determined the capacity of this compound to inhibit the adhesion of HUVEC to vitronectin, fibronectin, or osteopontin (Figure 6). Compound **18** suppressed the adhesion of IL-1β-stimulated HUVEC to vitronectin and osteopontin only partially (inhibition in the region of 50%), whereas a stronger suppression was found on fibronectin (inhibition in the region of 80%). This effect was at variance with the partial inhibition promoted by compound **18** on melanoma cell adhesion to fibronectin.

Effect of RGD Antagonists on in Vitro and in Vivo Angiogenesis. We examined the ability of compound **18** to repress angiogenesis by studying the tube formation by endothelial cells seeded on a Matrigel layer and the in vivo vessel invasion into Matrigel plugs. We found that compound **18** (final concentration of 0.1 μM) inhibited the tube formation by HUVEC seeded in Matrigel (Figure 7A). We confirmed

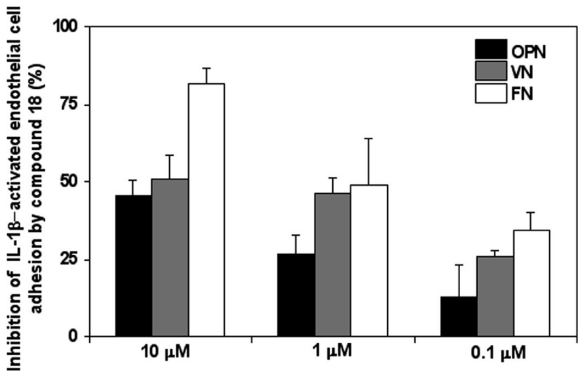

Figure 6. Inhibition values (%) of integrin-mediated IL-1β-stimulated HUVEC adhesion to osteopontin (OPN), vitronectin (VN), and fibronectin (FN) induced by compound **18**.

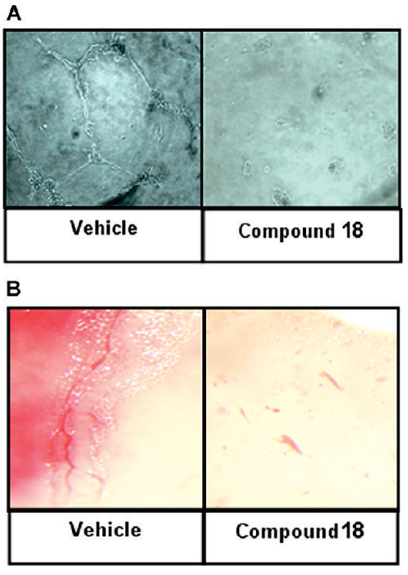

Figure 7. Inhibition of in vitro tube formation by HUVEC (A) and in vivo vessel invasion into Matrigel plugs (B), induced by compound **18**.

the in vitro antiangiogenic effect of compound **18**, demonstrating that this compound may inhibit vessel invasion into Matrigel plugs enriched in angiogenic growth factors, such as bFGF (Figure 7B).

Discussion

Cu-catalyzed Huisgen cycloaddition reaction between azides and alkynes bearing carboxylate and guanidino groups, respectively, allowed for the generation of a pool of triazole-based RGD mimetics, some of which showed binding affinity properties toward $\alpha_v\beta_3/\alpha_v\beta_5$ integrins. In particular, compound **18** was selected as a potent ligand for $\alpha_v\beta_3$ integrin. Molecular docking studies gave insight into a RGD-like binding mode of compound **18** toward $\alpha_v\beta_3$ integrin, also showing a peculiar π-stacking interaction between the triazole ring and Tyr178 side chain. Also, cluster analysis of docking calculations revealed two possible equilibrating conformations characterized by a π-stacking interaction between the aromatic ring of **18** and Tyr122 side chain and by a hydrogen bond between the Arg216 carbonyl group and the amide bond of **18**, respectively.

For cell biology experiments, we used A375M melanoma cells, a highly metastatic cell line expressing a variety of integrin receptors, which can adhere to fibronectin, osteopontin, and vitronectin with the same ability (data not shown). Metastatic tumor cells have redundant pathways to interact with cells and proteins of the extracellular matrix, including through the heparin binding domain also present on fibronectin, osteopontin, and vitronectin molecule. Thus, the suppression of tumor cell adhesion to a specific substrate by RGD antagonists might be sometimes incomplete. We showed that compound **18** inhibited the adhesion of human melanoma cells to extracellular matrix proteins, such as vitronectin, fibronection, and osteopontin. In particular, compound **18** proved to be more specific as an $\alpha_v\beta_3/\alpha_v\beta_5$ integrin antagonist in tumor cells, in view of the strong inhibition of the adhesion of A375M melanoma cells to vitronectin and osteopontin. The high affinity of compound **18** for $\alpha_v\beta_3/\alpha_v\beta_5$ was also revealed by the observation that compound **18** inhibited the adhesion of tumor cells to vitronectin only in the presence of Mn^{2+}, when integrins are in the activated form. A special interest was deserved on the capacity of compound **18** to inhibit tumor cell adhesion to osteopontin even at nanomolar concentration. Osteopontin represents a molecular biomarker of the invasion and dissemination in tumors of breast, stomach, lung, prostate, colon; moreover, the $\alpha_v\beta_3$/osteopontin interaction promotes the activation of osteoclasts, thus representing a possible mechanism of metastatic lytic lesions in bone,[24b] Compound **18** might have a role in the future in the diagnosis and treatment of bone metastases. Compound **18** also repressed the adhesion of IL-1β-stimulated HUVEC to vitronectin and osteopontin, although the most relevant inhibitory effect was found using fibronectin as a substrate. Furthermore, compound **18** blocked angiogenesis in in vitro and in vivo experimental models.

In conclusion, our results demonstrated that compound **18**, as a hit RGD mimetic, is capable of exerting relevant biological effects on integrin receptors associated with the plasma membrane of tumor cells (i.e., $\alpha_v\beta_3$, $\alpha_v\beta_5$) as well as endothelial cells, which is a requirement for its future applications as an antiangiogenic agent in anticancer diagnosis and therapeutic strategies.

Experimental Section

Combustion analysis was used to determine purity. All tested compounds were >95% pure.

General Click Chemistry and Hydrolysis Procedure for Compounds 9−22. To a stirred solution of alkyne (1 equiv) and azide (1 equiv) in H_2O/*t*-BuOH 1:1 (4 mL/mmol) were successively added a 0.9 M sodium ascorbate solution (1.1 mL/mmol, 1 equiv) and a 0.3 M solution of $Cu(OAc)_2$ (3 mL/mmol, 1 equiv). The mixture was stirred at room temperature for 2 days. The organic phase was extracted three times with CH_2Cl_2, washed with 5% $NaHCO_3$ solution and brine, then dried over Na_2SO_4, and evaporated. The crude mixture was purified through flash chromatography, thus obtaining the protected product in pure form. The title compounds were obtained as hydrochloride salts from the corresponding protected derivatives by acid catalyzed hydrolysis at room temperature for 16 h with 3 M HCl solution (5 mL/mmol).

{[2-(4-Guanidinomethyl[1,2,3]triazol-1-yl)acetyl]phenylamino}-acetic Acid Hydrochloride (9). Following the general procedure, alkyne **6** (165 mg, 0.55 mmol) and azide **1** (160 mg, 0.55 mmol) in H_2O/*t*-BuOH 1:1 (2 mL) gave, after workup and purification by flash chromatography (EtOAc/petroleum ether 2:1, R_f = 0.56), **Pg-9** (177 mg, 55%) as a yellow oil. ^{1}H NMR ($CDCl_3$, 200 MHz) δ 11.41 (br, 1 H), 8.71 (br, 1 H), 7.68 (s, 1 H), 7.40 (m, 5 H), 4.92 (s, 2 H), 4.66 (d, J = 6.0 Hz, 2 H), 4.23 (s, 2 H), 1.45 (s, 9 H), 1.42 (s, 9 H), 1.41 (s, 9 H). ^{13}C NMR ($CDCl_3$, 50 MHz) δ 167.1 (s), 164.9 (s), 163.0 (s), 155.6 (s), 152.5 (s), 143.4 (s), 140.5 (s), 130.0 (d, 2 C), 129.0 (d), 127.7 (d, 2 C), 123.7 (d), 82.9 (s), 82.1 (s), 79.0 (s), 52.2 (t), 50.9 (t), 36.2 (t), 28.1 (q, 3 C), 27.8 (q, 6 C). The hydrolysis of **Pg-9** allowed us to obtain the final product **9** as a pale orange solid. ^{1}H NMR (D_2O, 400 MHz) δ 7.76 (s, 1 H), 7.43−7.35 (m, 6 H), 5.11 (s, 2 H), 4.39 (s, 2 H), 4.36 (s, 2 H). ^{13}C NMR (D_2O, 50 MHz) δ 174.6 (s), 170.3 (s), 159.4 (s), 145.6 (s), 142.3 (s), 132.9 (d, 2C), 132.2 (d), 130.0 (d, 2 C), 128.0 (d), 54.5 (t), 54.3 (t), 38.8 (t). ESI-MSMS m/z 332 ($M - H^+$, 8.6), 315 (70), 245 (80), 199 (100). Anal. Calcd for $C_{14}H_{18}ClN_7O_3$: C, 45.72; H, 4.93; N, 26.66. Found: C, 45.81; H, 4.99; N, 26.54.

({2-[4-(2-Guanidinoethyl)[1,2,3]triazol-1-yl]acetyl}phenylamino)-acetic Acid Hydrochloride (10). Following the general procedure, alkyne **7** (200 mg, 0.64 mmol) and azide **1** (186 mg, 0.64 mmol) in H_2O/*t*-BuOH 1:1 (2.6 mL) gave, after workup and purification by flash chromatography (EtOAc/petroleum ether 4:1, R_f = 0.69), **Pg-10** (228 mg, 59%) as a white solid. ^{1}H NMR ($CDCl_3$, 200 MHz) δ 7.62 (s, 1 H), 7.44 (m, 5 H), 4.91 (s, 2 H), 4.27 (s, 2 H), 4.18 (t, J = 7.2 Hz, 2 H), 3.02 (t, J = 7.2 Hz, 2 H), 1.48 (s, 9 H), 1.46 (s, 9 H), 1.44 (s, 9 H). ^{13}C NMR ($CDCl_3$, 50 MHz) δ 167.1 (s), 165.1 (s), 163.1 (s), 160.0 (s), 154.6 (s), 143.2 (s), 140.7 (s), 130.1 (d, 2 C), 129.0 (d), 127.9 (d, 2 C), 123.3 (d), 83.9 (s), 82.2 (s), 78.7 (s), 52.4 (t), 50.9 (t), 44.3 (t), 28.4 (q, 3 C), 28.1 (q, 3 C), 28.0 (q, 3 C), 25.4 (t). The hydrolysis of **Pg-10** allowed us to obtain the final product **10** as a yellowish solid. ^{1}H NMR (D_2O, 400 MHz) δ 7.68 (s, 1 H), 7.44−7.37 (m, 5 H), 5.10 (s, 2 H), 4.38 (s, 2 H), 3.37 (t, J = 6.2 Hz, 2 H), 2.87 (t, J = 6.2 Hz, 2 H). ^{13}C NMR (D_2O, 50 MHz) δ 171.8 (s), 167.4 (s), 156.5 (s), 142.8 (s), 139.6 (s), 130.2 (d, 2 C), 129.5 (d), 127.3 (d, 3 C), 52.0 (t, 2 C), 40.4 (t), 24.2 (t). ESI-MSMS m/z 346 ($M - H^+$, 22), 329 (52), 301 (100). Anal. Calcd for $C_{15}H_{20}ClN_7O_3$: C, 47.18; H, 5.28; N, 25.68. Found: C, 47.24; H, 5.33; N, 25.53.

({2-[4-(3-Guanidinopropyl)[1,2,3]triazol-1-yl]acetyl}phenylamino)acetic Acid Hydrochloride (11). Following the general procedure, alkyne **8** (197 mg, 0.61 mmol) and azide **1** (176 mg, 0.61 mmol) in H_2O/*t*-BuOH 1:1 (2.4 mL) gave, after workup and purification by flash chromatography (EtOAc/petroleum ether 4:1, R_f = 0.75), **Pg-11** (232 mg, 62%) as a yellow oil. ^{1}H NMR ($CDCl_3$, 200 MHz) δ 9.30 (br, 2 H), 7.63 (s, 1 H), 7.48 (m, 5 H), 4.92 (s, 2 H), 4.27 (s, 2 H), 3.95 (t, J = 7.3 Hz, 2 H), 2.74 (t, J = 7.5 Hz, 2 H), 1.95 (m, 2 H), 1.48 (s, 9 H), 1.47 (s, 9 H), 1.43 (s, 9 H). ^{13}C NMR ($CDCl_3$, 50 MHz) δ 167.0 (s), 165.1 (s), 163.4 (s), 160.4 (s), 154.7 (s), 146.3 (s), 140.6 (s), 130.7 (d, 2 C), 129.0 (d), 127.8 (d, 2 C), 122.7 (d), 83.7 (s), 82.1 (s), 78.5 (s), 52.3 (t), 51.0 (t), 44.1 (t), 28.3 (q, 3 C), 28.1 (q, 3 C), 28.0 (q, 3 C), 23.0 (t), 21.8 (t). The hydrolysis of **Pg-11** allowed us to obtain the final product **10** as a yellow solid. ^{1}H NMR (D_2O, 400 MHz) δ 7.64 (s, 1 H), 7.44−7.36 (m, 5 H), 5.10 (s, 2 H), 4.38 (s, 2 H), 3.09 (t, J = 6.6 Hz, 2 H), 2.66 (t, J = 7.4 Hz, 2 H), 1.83 (m, 2 H). ^{13}C NMR (D_2O, 50 MHz) δ 174.7 (s), 170.3 (s), 159.4 (s), 142.3 (s),

139.6 (s), 132.9 (d, 2 C), 132.2 (d), 130.0 (d, 2 C), 128.1 (d), 54.6 (t, 2 C), 42.9 (t), 29.9 (t), 24.0 (t). ESI-MSMS m/z 360.2 ($M - H^+$, 0.6), 343 (54), 315 (16), 301 (26), 227 (100). Anal. Calcd for $C_{16}H_{22}ClN_7O_3$: C, 48.55; H, 5.60; N, 24.77. Found: C, 48.72; H, 5.64; N, 24.65.

[(2-{4-[2-(4-Carbamimidoylpiperazin-1-yl)ethyl][1,2,3]triazol-1-yl}acetyl)phenylamino]acetic Acid Hydrochloride (12). Following the general procedure, alkyne **5** (372 mg, 0.98 mmol) and azide **1** (284 mg, 0.98 mmol) in H_2O/*t*-BuOH 1:1 (4 mL) gave, after workup and purification by flash chromatography (CH_2Cl_2/MeOH 12:1, R_f = 0.46), **Pg-12** (450 mg, 68%) as an orange solid. ^{1}H NMR ($CDCl_3$, 200 MHz) δ 7.59 (s, 1 H), 7.45 (m, 5 H), 4.94 (s, 2 H), 4.28 (s, 2 H), 3.62 (m, 4 H), 2.90 (m, 2 H), 2.70 (m, 2 H), 2.57 (m, 4 H), 1.49 (s, 9 H), 1.47 (s, 9 H), 1.44 (s, 9 H). The hydrolysis of **Pg-12** gave the final product **12** as an orange solid. ^{1}H NMR (D_2O, 400 MHz) δ 7.88 (s, 1 H), 7.39−7.32 (m, 5 H), 5.06 (s, 2 H), 4.30 (m, 2 H), 3.94 (m, 2 H), 3.62 (m, 2 H), 3.51 (m, 2 H), 3.44 (m, 4 H), 3.12 (m, 4 H). ^{13}C NMR (D_2O, 50 MHz) δ 171.9 (s), 167.8 (s), 163.0 (s), 156.7 (s), 139.8 (s), 130.4 (d, 2 C), 129.7 (d), 127.5 (d, 3 C), 55.7 (t), 51.9 (t), 50.8 (t, 2 C), 48.7 (t), 42.7 (t, 2 C), 40.8 (t). ESI-MSMS m/z 415.2 ($M - H^+$, 16), 398 (69), 373 (36), 282 (100), 265 (15). Anal. Calcd for $C_{19}H_{27}ClN_8O_3$: C, 50.61; H, 6.04; N, 24.85. Found: C, 50.78; H, 6.08; N, 24.68.

(*R*)-3-[2-(4-Guanidinomethyl[1,2,3]triazol-1-yl)acetylamino]-3-phenylpropionic Acid Hydrochloride (13). Following the general procedure, alkyne **6** (301 mg, 1.01 mmol) and azide **3b** (308 mg, 1.01 mmol) in H_2O/*t*-BuOH 1:1 (4 mL) gave, after workup and purification by flash chromatography (EtOAc/petroleum ether 1:1, R_f = 0.25), **Pg-13** (273 mg, 45%) as a colorless oil. ^{1}H NMR ($CDCl_3$, 200 MHz) δ 11.42 (br, 1 H), 8.77 (t, J = 5.2 Hz, 1 H), 7.73 (s, 1 H), 7.48 (d, J = 8.0 Hz, 1 H), 7.30−7.16 (m, 5 H), 5.32 (m, 1 H), 5.02 (s, 2 H), 4.68 (d, J = 5.2 Hz, 2 H), 2.79 (m, 2 H), 1.45 (s, 9 H), 1.41 (s, 9 H), 1.29 (s, 9 H). ^{13}C NMR ($CDCl_3$, 50 MHz) δ 169.8 (s), 164.1 (s), 163.1 (s), 155.8 (s), 152.8 (s), 144.3 (s), 139.7 (s), 128.5 (d, 2 C), 127.6 (d), 126.1 (d, 2 C), 123.8 (d), 83.1 (s), 81.4 (s), 79.3 (s), 52.8 (t), 50.2 (d), 41.0 (t), 36.3 (t), 28.2 (q, 3 C), 27.9 (q, 3 C), 27.8 (q, 3 C). The hydrolysis of **Pg-13** gave the final product **13** as white solid. $[\alpha]^{24}_D$ +73.2 (c 0.23, H_2O). ^{1}H NMR (D_2O, 400 MHz) δ 7.86 (s, 1 H), 7.31−7.22 (m, 5 H), 5.15 (s, 2 H), 5.12 (t, J = 6.8 Hz, 2 H), 4.42 (s, 2 H), 2.64 (d, J = 6.8 Hz, 2 H). ^{13}C NMR (D_2O, 50 MHz) δ 180.4 (s), 169.4 (s), 159.5 (s), 145.9 (s), 143.5 (s), 131.4 (d, 2 C), 130.3 (d), 128.8 (d, 2 C), 127.7 (d), 54.8 (t), 54.6 (d), 45.6 (t), 38.9 (t). ESI-MSMS m/z 346 ($M - H^+$, 5.6), 329 (100), 304 (36), 259 (48). Anal. Calcd for $C_{15}H_{20}ClN_7O_3$: C, 47.18; H, 5.28; N, 25.68. Found: C, 47.26; H, 5.35; N, 25.57.

(*R*)-3-{2-[4-(2-Guanidinoethyl)[1,2,3]triazol-1-yl]acetylamino}-3-phenylpropionic Acid Hydrochloride (14). Following the general procedure, alkyne **7** (200 mg, 0.64 mmol) and azide **3a** (168 mg, 0.64 mmol) in H_2O/*t*-BuOH 1:1 (2.6 mL) gave, after workup and purification by flash chromatography (EtOAc/petroleum ether 4:1, R_f = 0.50), **Pg-14** (177 mg, 48%) as a yellow oil. ^{1}H NMR ($CDCl_3$, 200 MHz) δ 9.24 (br, 1 H), 7.68 (s, 1 H), 7.30−7.17 (m, 5 H), 5.38 (m, 1 H), 5.02 (s, 2 H), 4.17 (t, J = 7.3 Hz, 2 H), 3.58 (s, 3 H), 3.06 (t, J = 7.3 Hz, 2 H), 2.81 (m, 2 H), 1.49 (s, 9 H), 1.48 (s, 9 H). ^{13}C NMR ($CDCl_3$, 50 MHz) δ 170.7 (s), 164.3 (s), 163.5 (s), 160.0 (s), 154.5 (s), 145.6 (s), 139.5 (s), 128.6 (d, 2 C), 127.7 (d), 125.9 (d, 2 C), 123.3 (d), 84.0 (s), 78.7 (s), 52.9 (t), 51.9 (q), 50.1 (d), 44.2 (t), 39.7 (t), 28.5 (q, 3 C), 28.0 (q, 3 C), 25.4 (t). The hydrolysis of **Pg-14** allowed us to obtain the final product **14** as a yellow solid. $[\alpha]^{24}_D$ +60.9 (c 0.32, H_2O). ^{1}H NMR (D_2O, 400 MHz) δ 7.72 (s, 1 H), 7.32−7.28 (m, 5 H), 5.20 (m, 1 H), 5.14 (d, J = 5.2 Hz, 2 H), 3.38 (t, J = 6.4 Hz, 2 H), 3.89−2.85 (m, 4 H). ^{13}C NMR (D_2O, 50 MHz) δ 173.5 (s), 165.8 (s), 155.7 (s), 138.9 (s, 2 C), 128.0 (d, 2 C), 127.1 (d), 126.0 (d), 125.3 (d, 2 C), 51.3 (t), 49.8 (d), 39.4 (t), 38.9 (t), 23.3 (t). ESI-MSMS m/z 360.2 ($M - H^+$, 1.8), 343 (65), 315 (100). Anal. Calcd for $C_{16}H_{22}ClN_7O_3$: C, 48.55; H, 5.60; N, 24.77. Found: C, 48.70; H, 5.68; N, 24.65.

(*R*)-3-{2-[4-(3-Guanidinopropyl)[1,2,3]triazol-1-yl]acetylamino}-3-phenylpropionic Acid Hydrochloride (15). Following the general procedure, alkyne **8** (153 mg, 0.47 mmol) and azide **3a** (124 mg, 0.47 mmol) in H_2O/*t*-BuOH 1:1 (2 mL) gave, after workup and purification by flash chromatography (EtOAc/petroleum ether 4:1, R_f = 0.38), **Pg-15** (153 mg, 55%) as a yellow oil. ^{1}H NMR ($CDCl_3$, 200 MHz) δ 9.34 (br, 1 H), 7.28−7.20 (m, 6 H), 5.38 (m, 1 H), 5.05 (s, 2 H), 3.90 (m, 2 H), 3.55 (s, 3 H), 2.79 (m, 4 H), 1.98 (m, 2 H), 1.49 (s, 9 H), 1.46 (s, 9 H). ^{13}C NMR ($CDCl_3$, 50 MHz) δ 170.6 (s), 164.5 (s), 163.3 (s), 159.8 (s), 154.6 (s), 147.7 (s), 139.6 (s), 128.5 (d, 2 C), 127.5 (d), 126.0 (d, 2 C), 122.8 (d), 83.8 (s), 78.8 (s), 52.7 (t), 51.8 (q), 50.0 (d), 43.9 (t), 39.8 (t), 28.3 (q, 3 C), 28.0 (q, 3 C), 27.7 (t), 22.9 (t). The hydrolysis of **Pg-15** allowed us to obtain the final product **15** as a yellow solid. $[\alpha]^{24}_D$ +56.9 (c 0.39, H_2O). ^{1}H NMR (D_2O, 400 MHz) δ 7.68 (s, 1 H), 7.31−7.26 (m, 5 H), 5.19 (pt, J = 7.2 Hz, 1 H), 5.12 (d, J = 3.6 Hz, 2 H), 3.07 (t, J = 6.8, 2 H), 2.86 (d, J = 7.2 Hz, 2 H), 2.68 (t, J = 7.6 Hz, 2 H), 1.83 (m, 2 H). ^{13}C NMR (D_2O, 50 MHz) δ 177.0 (s), 168.8 (s), 159.2 (s), 142.4 (s, 2 C), 131.5 (d, 2 C), 130.7 (d), 129.6 (d), 128.8 (d, 2 C), 55.3 (t), 53.4 (d), 42.9 (t), 42.5 (t), 29.8 (t), 23.9 (t). ESI-MSMS m/z 374.2 ($M - H^+$, 1.8), 357 (100), 315 (82). Anal. Calcd for $C_{17}H_{24}ClN_7O_3$: C, 49.82; H, 5.90; N, 23.92. Found: C, 49.91; H, 5.97; N, 23.75.

(*S*)-3-[2-(4-Guanidinomethyl[1,2,3]triazol-1-yl)acetylamino]-3-phenylpropionic Acid Hydrochloride (16). Following the general procedure, alkyne **6** (195 mg, 0.66 mmol) and azide **2b** (200 mg, 0.66 mmol) in H_2O/*t*-BuOH 1:1 (2.6 mL) gave, after workup and purification by flash chromatography (EtOAc/petroleum ether 1:1, R_f = 0.25), **Pg-16** (388 mg, 64%). The hydrolysis of protected **Pg-16** compound gave the final product **16** as a yellowish solid with similar NMR data as reported for compound **13**. $[\alpha]^{24}_D$ −66.3 (c 0.2, H_2O). Anal. Calcd for $C_{15}H_{20}ClN_7O_3$: C, 47.18; H, 5.28; N, 25.68. Found: C, 47.29; H, 5.38; N, 25.59.

(*S*)-3-{2-[4-(2-Guanidinoethyl)[1,2,3]triazol-1-yl]acetylamino}-3-phenylpropionic Acid Hydrochloride (17). Following the general procedure, alkyne **7** (140 mg, 0.45 mmol) and azide **2a** (118 mg, 0.45 mmol) in H_2O/*t*-BuOH 1:1 (2 mL) gave, after workup and purification by flash chromatography (EtOAc/petroleum ether 4:1, R_f = 0.50), **Pg-17** (203 mg, 55%). The hydrolysis of protected **Pg-17** compound gave the final product **17** as a yellowish solid with similar NMR data as reported for compound **14**. $[\alpha]^{24}_D$ −63.2 (c 0.27, H_2O). Anal. Calcd for $C_{16}H_{22}ClN_7O_3$: C, 48.55; H, 5.60; N, 24.77. Found: C, 48.72; H, 5.69; N, 24.64.

(*S*)-3-{2-[4-(3-Guanidinopropyl)[1,2,3]triazol-1-yl]acetylamino}-3-phenylpropionic Acid Hydrochloride (18). Following the general procedure, alkyne **8** (200 mg, 0.61 mmol) and azide **2a** (160 mg, 0.61 mmol) in H_2O/*t*-BuOH 1:1 (2.5 mL) gave, after workup and purification by flash chromatography (EtOAc/petroleum ether 4:1, R_f = 0.38), **Pg-18** (215 mg, 60%). The hydrolysis of protected **Pg-18** compound gave the final product **18** as a yellowish solid with similar NMR data as reported for compound **15**. $[\alpha]^{24}_D$ −63.5 (c 0.57, H_2O). Anal. Calcd for $C_{17}H_{24}ClN_7O_3$: C, 49.82; H, 5.90; N, 23.92. Found: C, 49.90; H, 5.94; N, 23.71.

(*R*)-3-{2-[4-(4-Carbamimidoylpiperazin-1-ylmethyl)[1,2,3]triazol-1-yl]acetylamino}-3-phenylpropionic Acid Hydrochloride (19). Following the general procedure, alkyne **4** (117 mg, 0.32 mmol) and azide **3b** (98 mg, 0.32 mmol) in H_2O/*t*-BuOH 1:1 (1.5 mL) gave, after workup and purification by flash chromatography (CH_2Cl_2/MeOH 10:1, R_f = 0.47), **Pg-19** (93 mg, 43%) as a yellowish oil. ^{1}H NMR ($CDCl_3$, 200 MHz) δ 7.63 (s, 1H), 7.37 (br, 1 H), 7.20 (m, 5 H), 5.33 (m, 1 H), 5.01 (s, 2 H), 3.65 (s, 2 H), 3.51 (m, 4 H), 2.68 (m, 2 H), 2.51 (m, 4 H), 1.46 (s, 18 H), 1.28 (s, 9 H). ^{13}C NMR ($CDCl_3$, 50 MHz) δ 169.7 (s), 164.1 (s), 162.8 (s), 154.4 (s), 144.0 (s), 139.7 (s), 137.2 (s), 128.3 (d, 2 C), 127.5 (d), 126.1 (d, 2 C), 124.3 (d), 88.7 (s), 81.2 (s), 80.0 (s), 52.6 (t), 52.4 (t), 52.1 (t), 50.2 (d), 46.4 (t), 41.0 (t), 28.2 (q), 27.9 (q, 3 C), 27.6 (q, 3 C). The hydrolysis of **Pg-19** allowed us to obtain the final

product **19** as a white solid. $[\alpha]^{24}_D$ +49.3 (*c* 0.21, H_2O). ^1H NMR (D_2O, 400 MHz) δ 7.96 (s, 1 H), 7.33−7.27 (m, 5 H), 5.23 (s, 2 H), 5.17 (t, J = 6.8 Hz, 2 H), 3.87 (s, 2 H), 3.45 (m, 4 H), 3.21 (m, 2 H), 2.67 (m, 4 H). ^{13}C NMR (D_2O, 50 MHz) δ 180.9 (s), 169.2 (s), 158.8 (s), 143.7 (s), 143.4 (s), 131.4 (d, 2 C), 130.3 (d), 129.7 (d), 128.8 (d, 2 C), 54.8 (t), 52.9 (t), 50.8 (d), 47.0 (t), 46.2 (t), 45.6 (t). ESI-MSMS m/z 415 ($M - H^+$, 32), 398 (27), 373 (100). Anal. Calcd for $C_{19}H_{27}ClN_8O_3$: C, 50.61; H, 6.04; N, 24.85. Found: C, 50.71; H, 6.11; N, 24.43.

(*R*)-3-(2-{4-[2-(4-Carbamimidoylpiperazin-1-yl)ethyl][1,2,3]triazol-1-yl}acetylamino)-3-phenylpropionic Acid Hydrochloride (20). Following the general procedure, alkyne **5** (319 mg, 0.84 mmol) and azide **3a** (221 mg, 0.84 mmol) in H_2O/*t*-BuOH 1:1 (3.5 mL) gave, after workup and purification by flash chromatography (CH_2Cl_2/MeOH 12:1, R_f = 0.46), **Pg-20** (297 mg, 55%). ^1H NMR ($CDCl_3$, 200 MHz) δ 7.54 (s, 1 H), 7.30−7.20 (m, 5 H), 5.38 (m, 1 H), 5.03 (s, 2 H), 3.58 (m, 4 H), 3.58 (s, 3 H), 2.94 (m, 2 H), 2.81 (m, 2 H), 2.71 (m, 2 H), 2.56 (m, 4 H), 1.48 (s, 18 H). ^{13}C NMR ($CDCl_3$, 50 MHz) δ 170.8 (s), 164.4 (s), 162.8 (s), 154.6 (s), 146.4 (s), 139.5 (s), 137.2 (s), 128.6 (d, 2 C), 127.7 (d), 126.0 (d, 2 C), 122.8 (d), 88.7 (s), 81.2 (s), 57.3 (t), 52.9 (t), 52.5 (t), 52.0 (q), 50.0 (d), 46.8 (t), 39.7 (t), 28.2 (q, 6C), 23.3 (t). The hydrolysis of **Pg-20** gave the final product **20** as a white solid. $[\alpha]^{24}_D$ +57.4 (*c* 0.31, H_2O). ^1H NMR (D_2O, 400 MHz) δ 7.81 (s, 1 H), 7.33−7.28 (m, 5 H), 5.18−5.16 (m, 3 H), 3.68 (m, 4 H), 3.54−3.41 (m, 6 H), 3.16 (t, J = 7.4 Hz, 2 H), 2.84 (d, J = 7.2 Hz, 2 H). ^{13}C NMR (D_2O, 50 MHz) δ 173.5 (s), 165.9 (s), 155.6 (s), 141.3 (s), 138.9 (s), 128.0 (d, 2 C), 127.1 (d), 125.3 (d, 2 C), 124.7 (d), 54.7 (t), 51.2 (d), 49.8(t), 41.6 (t), 39.7 (t), 38.9 (t), 18.9 (t). ESI-MSMS m/z 429.2 ($M - H^+$, 33), 413 (100), 388 (30). Anal. Calcd for $C_{20}H_{29}ClN_8O_3$: C, 51.66; H, 6.29; N, 24.10. Found: C, 51.78; H, 6.34; N, 24.01.

(*S*)-3-{2-[4-(4-Carbamimidoylpiperazin-1-ylmethyl)[1,2,3]triazol-1-yl]acetylamino}-3-phenylpropionic Acid Hydrochloride (21). Following the general procedure, alkyne **4** (222 mg, 0.61 mmol) and azide **2b** (186 mg, 0.61 mmol) in H_2O/*t*-BuOH 1:1 (2 mL) gave, after workup and purification by flash chromatography (CH_2Cl_2/MeOH 10:1, R_f = 0.47), **Pg-21** (201 mg, 49%). The hydrolysis of protected **Pg-21** compound gave the final product **21** as a yellowish solid with similar NMR data as reported for compound **19**. $[\alpha]^{24}_D$ −70.8 (*c* 0.58, H_2O). Anal. Calcd for $C_{19}H_{27}ClN_8O_3$: C, 50.61; H, 6.04; N, 24.85. Found: C, 50.69; H, 6.13; N, 24.38.

(*S*)-3-(2-{4-[2-(4-Carbamimidoylpiperazin-1-yl)ethyl][1,2,3]triazol-1-yl}acetylamino)-3-phenylpropionic Acid Hydrochloride (22). Following the general procedure, alkyne **5** (361 mg, 0.95 mmol) and azide **2a** (250 mg, 0.95 mmol) in H_2O/*t*-BuOH 1:1 (4 mL) gave, after workup and purification by flash chromatography (CH_2Cl_2/MeOH 12:1, R_f = 0.46), **Pg-22** (400 mg, 65%). The hydrolysis of protected **Pg-22** compound gave the final product **22** as a yellow solid with similar NMR data as reported for compound **20**. $[\alpha]^{24}_D$ −55.2 (*c* 0.32, H_2O). Anal. Calcd for $C_{20}H_{29}ClN_8O_3$: C, 51.66; H, 6.29; N, 24.10. Found: C, 51.73; H, 6.36; N, 24.00.

Integrin Binding Assay. [^{125}I]Echistatin, labeled by the lactoperoxidase method[25] to a specific activity of 2200 Ci/mmol, was purchased from PerkinElmer Life Sciences, Boston, MA. Integrin proteins $\alpha_v\beta_3$ and $\alpha_v\beta_5$ purified from human placenta were purchased from Chemicon International Inc., Temecula, CA. The receptor binding assay was performed as described.[16] Purified receptors $\alpha_v\beta_3$ and $\alpha_v\beta_5$ were diluted respectively at 500 and 1000 ng/mL in a coating buffer [20 mM Tris (pH 7.4), 150 mM NaCl, 2 mM $CaCl_2$, 1 mM $MgCl_2$, 1 mM $MnCl_2$]. An aliquot of the diluted receptors (100 μL/well) was added to a 96-well microtiter plate (Optiplate-96 HB, PerkinElmer Life Sciences, Boston, MA) and incubated overnight at 4 °C. The plate was washed once with a blocking/binding buffer [20 mM Tris (pH 7.4), 150 mM NaCl, 2 mM $CaCl_2$, 1 mM $MgCl_2$, 1 mM $MnCl_2$, 1% BSA] and incubated for an additional 2 h at room temperature. The plate was rinsed twice with the same buffer, and then competition binding studies were performed with a fixed concentration of [^{125}I]echistatin (0.05 and 0.1 nM for $\alpha_v\beta_3$ and $\alpha_v\beta_5$, respectively) and concentrations ranging from 0.01 nM to 100 μM tested compounds. All assays were performed in triplicate in a final volume of 0.2 mL, each containing the following species: 0.05 mL of [^{125}I]echistatin, 0.04 mL of the tested compound, and 0.11 mL of the blocking/binding buffer. Nonspecific binding was defined as [^{125}I]echistatin bound in the presence of an excess (1 μM) of unlabeled echistatin. After 3 h incubating at room temperature, the plate was washed three times with the blocking/binding buffer. Then it was counted in a Top-Count NXT microplate scintillation counter (PerkinElmer Life Sciences, Boston, MA) using 200 μL/well of MicroScint-40 liquid scintillation (PerkinElmer Life Sciences, Boston, MA). The IC_{50} values were determined by fitting the binding inhibition data by nonlinear regression using GraphPad Prism 4.0 software package (GraphPad Prism, San Diego, CA). Moreover, when the Hill slope of the curves was significantly less than unity ($K < -0.80$), the data were reprocessed with a two-sites model. The displacement curves that fitted ($p < 0.05$) better according to a two-sites model rather than to a one-site model were considered significant.

Cell Lines and Culture Conditions. A375P and A375M human melanoma cell lines used in this study were obtained from American Type Culture Collection (ATCC, Rockville, MD). The A375M cells were a clone isolated in hard agarose by Li et al.[23] from A375P cells and characterized by a high lung metastatic potential. Melanoma cells were grown in Dulbecco's modified Eagle medium containing 4500 mg/L glucose (DMEM 4500, GIBCO) supplemented with 10% fetal calf serum (FCS) at 37 °C in a humidified incubator containing 10% CO_2. Then 5.0×10^5 cells were seeded in 100 mm Sarstedt dishes and propagated every 3 days by incubation with a trypsin−EDTA solution. The capacity of A375M cells to grow in dense agarose was evaluated before the experiments. Cultures were periodically monitored for mycoplasma contamination .

Primary cultures of human umbilical vein endothelial cells (HUVEC) were obtained from Lonza. Cells grown in an endothelial cell growth medium-2 (EGM-2) containing endothelial cell growth supplements were subcultivated using a trypsin−EDTA solution, 1:3 split ratio. For the use in the experiments, cells (passages 2−4) were grown to confluence in plates coated with 1% bovine gelatin.

RNA Isolation and Polymerase Chain Reaction (PCR). Total RNA extracted using RNAgents (Total RNA Isolation System, Promega, Madison, WI) was determined spectrophotometrically. Complementary DNA (cDNA) was synthesized from 2 μg of total RNA using 1 μL of ImProm-II reverse transcriptase (Promega). Aliquots of 2 μL of the cDNA were used for PCR amplification. The specific primers used for the identification of human α_v, α_5, β_1, β_3, β_5, and GAPDH are reported in Table S1 of Supporting Informations. All PCR experiments were conducted using 0.05 U/μL Go-Taq polymerase (Promega). Amplification was carried out on a Perkin-Elmer thermal cycler. An amount of 8 μL of each PCR product was visualized by a 2% agarose gel containing ethidium bromide (0.5 μg/mL) electrophoresis. cDNA products were evaluated on the basis of a standard PCR marker.

Flow Cytometry Assay. Cells were detached by gentle treatment with Accutase, a 0.5 mM EDTA solution, washed, and incubated for 1 h at 4 °C in the presence of anti-$\alpha_v\beta_3$ monoclonal antibody (1 μg/50 μL, anti-integrin $\alpha_v\beta_3$, clone LM609, Millipore). Cells were then washed and incubated for 1 h at 4 °C with a secondary antibody, 5 μg/mL goat antimouse IgG conjugated with FITC (Santa Cruz Biotecnology, Inc., Santa Cruz, CA). $\alpha_v\beta_3$-Positive cells were analyzed at 488 nm on the flow cytometer FACScan system (BD-FACS Canto).

Cell Adhesion Assay. Plates (96 wells) were coated with fibronectin (1 μg/mL), osteopontin (0.5 μg/mL), or vitronectin (10 μg/mL) by overnight incubation at 4 °C. Plates were washed

with PBS and then incubated at 37 °C for 1 h with PBS−1% BSA. After being washed, tumor cells or IL-1β (400 U/mL) stimulated HUVEC were counted, resuspended in serum free medium, and exposed to compound **18** (final concentration of compound was 0.1, 1, or 10 μM) at 37 °C for 30 min to allow the ligand−receptor equilibrium to be reached. In the case of melanoma cell adhesion, assays were performed in the presence or in the absence of 2 mM $MnCl_2$ solution.[26] Cells were plated ($(4-5)\times10^4$ cells/well) and incubated at 37 °C for 2 h. All the wells were washed with PBS to remove the nonadherent cells, and 0.5% crystal violet solution in 20% methanol was added. After 2 h of incubation at 4 °C, plates were examined at 540 nm in a counter ELX800 (Bio TEK Instruments). Experiments were conducted in triplicate and were repeated at least three times.

In Vitro Tubular Formation by HUVEC. Matrigel (10 μg/μL, BD Bioscience, San Jose, CA) precoated 96-well plates were used, and HUVEC (20 000 cells/well) were seeded in the presence of compound **18** (10 μM final concentration). Cells were incubated at 37 °C for 16−18 h, and capillary-like tube structures were examined and photographed by the use of a Nikon inverted microscope. The experiments were repeated three times.

In Vivo Angiogenesis Assay. The 5- to 6-week-old C57Bl/6 mice were used. Matrigel solution was mixed with 50 U/mL heparin resuspended in EGM-2 medium and compound **18**. Compound **18** was used at the final concentration of 0.1 μM. 500 μL Matrigel mixture was injected subcutaneously, and 5 days after, mice were sacrificed. Matrigel plugs were removed and photographed with the aid of a dissecting microscope.

Acknowledgment. Financial support from Istituto Toscano Tumori, MIUR (PRIN08, Grant 2008J4YNJY_003), and Fondazione Roma is acknowledged.

Supporting Information Available: Experimental procedures for compounds **1**−**8**; ^{1}H and ^{13}C NMR spectra of compounds **9**−**22**; inhibition curves of [^{125}I]echistatin specific binding to purified human integrin proteins $\alpha_V\beta_3$ and $\alpha_V\beta_5$ by compounds **15**, **16**, **17**, **20**, and **22**; and Table S1 detailing specific primers for the identification of human αv, α5, β1, β3, β5, and GAPDH. This material is available free of charge via the Internet at http://pubs.acs.org.

References

(1) For reviews, see the following: (a) Arnaout, M. A.; Goodman, S. L.; Xiong, J. P. Coming to grips with integrin binding to ligands. *Curr. Opin. Cell Biol.* **2002**, *14*, 641–651. (b) Hynes, R. O. Integrins: bidirectional, allosteric signaling machines. *Cell* **2002**, *110*, 673–687. (c) Plow, E. F.; Haas, T. A.; Zhang, L.; Loftus, J.; Smith, J. W. Ligand binding to integrins. *J. Biol. Chem.* **2000**, *275*, 21785–21788. (d) Humphries, M. J. Integrin structure. *Biochem. Soc. Trans.* **2000**, *28*, 311–339.

(2) Ruoslathi, E.; Pierschbacher, M. D. New perspectives in cell adhesion: RGD and integrins. *Science* **1987**, *238*, 491–497.

(3) For $\alpha_v\beta_3$, see the following: (a) Eliceiri, B. P.; Cheresh, D. A. Role of αv integrins during angiogenesis. *Cancer J.* **2000**, *13*, 245–249. (b) Burke, P. A.; De Nardo, S. J.; Miers, L. A.; Lamborn, K. L.; Matzku, S.; De Nardo, G. L. Cilengitide targeting of $\alpha_v\beta_3$ integrin receptor synergizes with radioimmunotherapy to increase efficacy and apoptosis in breast cancer xenografts. *Cancer Res.* **2002**, *62*, 4263–4272. (c) Haubner, R.; Finsinger, D.; Kessler, H. Stereoisomeric peptide libraries and peptidomimetics for designing selective inhibitors of the alpha-(V)beta(3) integrin for a new cancer therapy. *Angew. Chem., Int. Ed. Engl.* **1997**, *36*, 1374–1389. For $\alpha_v\beta_5$, see the following: (d) Marinelli, L.; Gottschalk, K. E.; Meyer, A.; Novellino, E.; Kessler, H. Human integrin αvβ5: homology modeling and ligand binding. *J. Med. Chem.* **2004**, *47*, 4166–4177. (e) Friedlander, M.; Theesfeld, C. L.; Sugita, M.; Fruttiger, M.; Thomas, M. A.; Chang, S.; Cheresh, D. Involvement of integrins alpha v beta 3 and alpha v beta 5 in ocular neovascular diseases. A. *Proc. Natl. Acad. Sci. U.S.A.* **1996**, *93*, 9764–9769. (f) Friedlander, M.; Brooks, P. C.; Shaffer, R. W.; Kincaid, C. M.; Varner, J. A.; Cheresh, D. A. Definition of two angiogenic pathways by distinct alpha v integrins. *Science* **1995**, *270*, 1500–1502.

(4) Mitjans, F.; Meyer, T.; Fittschen, C.; Goodman, S.; Jonczyk, A.; Marshall, J. F.; Reyes, G.; Piulats, J. In vivo therapy of malignant melanoma by means of antagonists of alphav integrins. *Int. J. Cancer* **2000**, *87*, 716–723.

(5) MacDonald, T. J.; Taga, T.; Shimada, H.; Tabrizi, P.; Zlokovic, B. V.; Cheresh, D. A.; Laug, W. E. Preferential susceptibility of brain tumors to the antiangiogenic effects of an alpha 31(v) integrin antagonist. *Neurosurgery* **2001**, *48*, 151–157.

(6) Albelda, S. M.; Mette, S. A.; Elder, D. E.; Stewart, R.; Damjanovich, L.; Herlyn, M.; Buck, C. A. Integrin distribution in malignant melanoma: association of the beta 3 subunit with tumor progression. *Cancer Res.* **1990**, *50*, 6757–6764.

(7) (a) Van Belle, P. A.; Elenitsas, R.; Satyamoorthy, K.; Wolfe, J. T.; Guerry, D., IV; Schuchter, L.; Van Belle, T. J.; Albelda, S.; Tahin, P.; Herlyn, M.; Elder, D. E. Progression-related expression of beta3 integrin in melanomas and nevi. *Hum. Pathol.* **1999**, *30*, 562–567. (b) Seftor, R. E. Role of the beta3 integrin subunit in human primary melanoma progression: multifunctional activities associated with alpha(v)beta3 integrin expression. *Am. J. Pathol.* **1998**, *153*, 1347–1351.

(8) (a) McGary, E. C.; Lev, D. C.; Bar-Eli, M. Cellular adhesion pathways and metastatic potential of human melanoma. *Cancer Biol. Ther.* **2002**, *1*, 459–465. (b) Hofmann, U. B.; Westphal, J. R.; Waas, E. T.; Becker, J. C.; Ruiter, D. J.; van Muijen, G. N. Coexpression of integrin alpha(v)beta3 and matrix metalloproteinase-2 (MMP-2) coincides with MMP-2 activation: correlation with melanoma progression. *J. Invest. Dermatol.* **2000**, *115*, 625–632.

(9) (a) Cai, W.; Chen, X. Anti-angiogenic cancer therapy based on integrin $\alpha_v\beta_3$ antagonism. *Anti-Cancer Agents Med. Chem.* **2006**, *6*, 407–428. (b) Kerbel, R.; Folkman, J. Clinical translation of angiogenesis inhibitors. *Nat. Rev. Cancer.* **2002**, *2*, 727–739. (c) Folkman, J. Angiogenesis: an organizing principle for drug discovery? *Nat. Rev. Drug Discovery* **2007**, *6*, 273–286. (d) Brooks, P. C.; Stromblad, S.; Klemke, R.; Visscher, D.; Sarkar, F. H.; Cheresh, D. A. The role of αv integrins during angiogenesis: insights into potential mechanisms of action and clinical development. *J. Clin. Invest.* **1995**, *96*, 1815–1822. (e) Kumar, C. C.; Malkowski, M.; Yin, Z.; Tanghetti, E.; Yaremko, B.; Nechuta, T.; Varner, J.; Liu, M.; Smith, E. M.; Neustadt, B.; Presta, M.; Armstrong, L. *Cancer Res.* **2001**, *61*, 2232–2238.

(10) (a) Raboisson, P.; DesJarlais, R. L.; Reed, R.; Lattanze, J.; Chaikin, M.; Manthey, C. L.; Tomczuk, B. E.; Marugán, J. J. Identification of novel short chain 4-substituted indoles as potent $\alpha_v\beta_3$ antagonist using structure-based drug design. *Eur. J. Med. Chem.* **2007**, *42*, 334–343. (b) Ishikawa, M.; Kubota, D.; Yamamoto, M.; Kuroda, C.; Iguchi, M.; Koyanagi, A.; Murakami, S.; Ajito, K. Tricyclic pharmacophore-based molecules as novel integrin $\alpha_v\beta_3$ antagonists. Part 2: Synthesis of potent $\alpha_v\beta_3/\alpha_{IIb}\beta_3$ dual antagonists. *Bioorg. Med. Chem.* **2006**, *14*, 2109–2130. (c) Cacciari, B.; Spalluto, G. Non peptidic $\alpha_v\beta_3$ antagonists: recent developments. *Curr. Med. Chem.* **2005**, *12*, 51–70.

(11) (a) Bach, A. C., II; Espina, J. R.; Jackson, S. A.; Stouten, P. F. W.; Duke, J. L.; Mousa, S. A.; DeGrado, W. F. Type II′ to type I β-turn swap changes specificity for integrins. *J. Am. Chem. Soc.* **1996**, *118*, 293–294. (b) Dechantsreiter, M.; Plnaker, E.; Mathä, B.; Lohof, E.; Hölzemann, G.; Jonczyk, A.; Goodman, S. L.; Kessler, H. N-Methylated cyclic RGD peptides as highly active and selective αvβ3 integrin antagonists. *J. Med. Chem.* **1999**, *42*, 3033–3040. (c) Lohof, E.; Plnaker, E.; Mang, C.; Burkhart, F.; Dechantsreiter, M. A.; Haubner, R.; Wester, H. J.; Schwaiger, M.; Hölzemann, G.; Goodman, S. L.; Kessler, H. Carbohydrate derivatives for use in drug design: cyclic α_v-selective RGD peptides. *Angew. Chem., Int. Ed.* **2000**, *39*, 2761–2764. (d) Belvisi, L.; Bernardi, A.; Checchia, A.; Manzoni, L.; Potenza, D.; Scolastico, C.; Castorina, M.; Capelli, A.; Giannini, G.; Carminati, P.; Pisano, C. Potent integrin antagonists from a small library of RGD-including cyclic pseudopeptides. *Org. Lett.* **2001**, *3*, 1001–1004. (e) Casiraghi, G.; Rassu, G.; Auzzas, L.; Bureddu, P.; Gaetani, E.; Battistini, L.; Zanardi, F.; Curti, C.; Nicastro, G.; Belvisi, L.; Motto, I.; Castorina, M.; Giannini, G.; Pisano, C. Grafting aminocyclopentane carboxylic acids onto the RGD tripeptide sequence generates low nanomolar $\alpha_v\beta_3/\alpha_v\beta_5$ integrin dual binders. *J. Med. Chem.* **2005**, *48*, 7675–7687. (f) Belvisi, L.; Bernardi, A.; Colombo, M.; Manzoni, L.; Potenza, D.; Scolastico, C.; Giannini, G.; Marcellini, M.; Riccioni, T.; Castorina, M.; Lo Giudice, P.; Carminati, P.; Pisano, C. Targeting integrins: insights into structure and activity of cyclic RGD pentapeptide mimics containing azabicycloalkane amino acids. *Bioorg. Med. Chem.* **2006**, *14*, 169–180.

(12) For reviews, see the following: (a) Arkin, M. R.; Wells, J. A. Small-molecule inhibitors of protein−protein interactions: progressing towards the dream. *Nat. Rev. Drug Discovery* **2004**, *3*, 301–317. (b) Szczepankiewicz, B. G.; Liu, G.; Jajduk, P. J.; Abad-Zapatero, C.; Pei, Z.; Xin, Z.; Lubben, T. H.; Trevillyan, J. M.; Stashko, M. A.; Ballaron, S. J.; Liang, H.; Huang, F.; Hutchings, C. W.; Fesik, S. W.; Jirousek,

M. R. Discovery of a potent, selective protein tyrosine phosphatase 1B inhibitor using a linked-fragment strategy. *J. Am. Chem. Soc.* **2003**, *125*, 4087–4096. (c) Erlanson, D. A.; Braisted, A. C.; Raphael, D. R.; Randal, M.; Stroud, R. M.; Gordon, E. M.; Wells, J. Site-directed ligand discovery. *Proc. Natl. Acad. Sci. U.S.A.* **2000**, *97*, 9367–9372. (d) Birk, A.; Lin, Y.-C.; Elder, J.; Wong, C.-H. A quick diversity-oriented amide-forming reaction to optimize P-subsite residues of HIV protease inhibitors. *Chem. Biol.* **2002**, *9*, 891–896.

(13) Kolb, H. C.; Sharpless, K. B. The growing impact of click chemistry on drug discovery. *Drug Discovery Today* **2003**, *8*, 1128–1137.

(14) (a) Wu, C. -Y.; Jan, J.-T.; Ma, S.-H.; Kuo, C.-J.; Juan, H.-F.; Cheng, Y.-S. E.; Hsu, H.-H.; Huang, H.-C.; Wu, D.; Brik, A.; Liang, F.-S.; Liu, R.-S.; Fang, J.-M.; Chen, S.-T.; Liang, P.-H.; Wong, C.-H. Small molecules targeting severe acute respiratory syndrome human coronavirus. *Proc. Natl. Acad. Sci. U.S.A.* **2004**, *101*, 10012–10017. (b) Wu, C.-Y.; Chang, C.-F.; Chen, J. S.-Y.; Wong, C.-H. Rapid diversity-oriented synthesis in microtiter plates for in situ screening: discovery of potent and selective α-fucosidase inhibitors. *Angew. Chem., Int. Ed.* **2003**, *42*, 4661–4664. (c) Best, M. D.; Birk, A.; Chapman, E.; Lee, L. V.; Cheng, W.-C.; Wong, C.-H. Rapid discovery of potent sulfotransferase inhibitors by diversity-oriented reaction in microplates followed by in situ screening. *ChemBioChem* **2004**, *5*, 811–819. (d) Lee, L. V.; Mitchell, M. L.; Huang, S.-J.; Fokin, V. V.; Sharpless, K. B.; Wong, C.-H. A potent and highly selective inhibitor of human α-1,3-fucosyltransferase via click chemistry. *J. Am. Chem. Soc.* **2003**, *125*, 9588–9589.

(15) (a) Belkin, V. M.; Belkin, A. M.; Koteliansky, V. E. Human smooth muscle VLA-1 integrin: purification, substrate specificity, localization in aorta, and expression during development. *J. Cell Biol.* **1990**, *111*, 2159–2170. (b) Pytela, R.; Pierschbacher, M. D.; Argraves, S.; Suzuki, S.; Ruoslahti, E. Arginine−glycine−aspartic acid adhesion receptors. *Methods Enzymol.* **1987**, *144*, 475–489.

(16) (a) Kumar, C. C.; Malkowski, M.; Yin, Z.; Tanghetti, E.; Yaremko, B.; Nechuta, T.; Varner, J.; Liu, M.; Smith, E. M.; Neustadt, B.; Presta, M.; Armstrong, L. Inhibition of angiogenesis and tumor growth by SCH221153, a dual alpha(v)beta3 and alpha(v)beta5 integrin receptor antagonist. *Cancer Res.* **2001**, *61*, 2232–2238. (b) Kumar, C. C.; Nie, H.; Rogers, C. P.; Malkowski, M.; Maxwell, E.; Catino, J. J.; Armstrong, L. Biochemical characterization of the binding of echistatin to integrin $\alpha_v\beta_3$ receptor. *J. Pharmacol. Exp. Ther.* **1997**, *283*, 843–853.

(17) (a) Dijkgraaf, I.; Kruijtzer, J. A.; Frielink, C.; Soede, A. C.; Hilbers, H. W.; Oyen, W. J.; Corstens, F. H.; Liskamp, R. M.; Boerman, O. C. Synthesis and biological evaluation of potent alphavbeta3-integrin receptor antagonists. *Nucl. Med. Biol.* **2006**, *33*, 953–961. (b) Zanardi, F.; Burreddu, P.; Rassu, G.; Auzzas, L.; Battistini, L.; Curti, C.; Sartori, A.; Nicastro, G.; Menchi, G.; Cini, N.; Bottoncetti, A.; Raspanti, S.; Casiraghi, G. Discovery of subnanomolar arginine-glycine-aspartate-based $\alpha_v\beta_3/\alpha_v\beta_5$ integrin binders embedding 4-amino-proline residues. *J. Med. Chem.* **2008**, *51*, 1771–1782.

(18) (a) Takagi, J.; Petre, B. M.; Walz, T.; Springer, T. A. Global conformational rearrangements in integrin extracellular domains in outside-in and inside-out signaling. *Cell* **2002**, *110*, 599–611. (b) Humphries, M. J.; McEwan, P. A.; Barton, S. J.; Buckley, P. A.; Bella, J.; Mould, A. P. Integrin structure: heady advances in ligand binding, but activation still makes the knees wobble. *Trends Biochem. Sci.* **2003**, *28*, 313–320.

(19) Shimaoka, M.; Springer, T. A. Therapeutic antagonists and conformational regulation of integrin function. *Nat. Rev. Drug Discovery* **2003**, *2*, 703–716.

(20) Xiong, J. P.; Stehle, T.; Zhang, R.; Joachimiak, A.; Frech, M.; Goodman, S. L.; Arnaout, M. A. Crystal structure of the extracellular segment of integrin v3 in complex with an Arg-Gly-Asp ligand. *Science* **2002**, *296*, 151–155.

(21) Bednar, R. A.; Gaul, S. L.; Hamill, T. G.; Egbertson, M. S.; Shafer, J. A.; Hartman, G. D.; Gould, R. J.; Bednar, B. Identification of low molecular weight GP IIb/IIIa antagonists that bind preferentially to activated platelets. *J. Pharmacol. Exp. Ther.* **1998**, *285*, 1317–1326.

(22) (a) Morris, G. M.; Goodsell, D. S.; Halliday, R. S.; Huey, R.; Hart, W. E.; Belew, R. K.; Olson, A. J. Automated docking using a Lamarckian genetic algorithm and an empirical binding free energy function. *J. Comput. Chem.* **1998**, *19*, 1639–1662. (b) Autodock results were processed using the PyMOL software: DeLano, W. L. *The PyMOL Molecular Graphics System*, version 0.99; DeLano Scientific LLC: San Carlos, CA; http://www.pymol.org.

(23) Li, L.; Price, J. E.; Fan, D.; Zhang, R. D.; Bucana, C. D.; Fidler, I. J. Correlation of growth capacity of human tumor cells in hard agarose with their in vivo proliferative capacity at specific metastatic sites. *J. Natl. Cancer Inst.* **1989**, *81*, 1406–1412.

(24) (a) Shattil, S. J.; Kim, C.; Ginsberg, M. H. The final step of integrin activation: the end game. *Nat. Rev. Mol. Cell Biol.* **2010**, *11*, 288–300. (b) Wai, P. Y.; Kuo, P. C. Osteopontin: regulation in tumor metastasis. *Cancer Metastasis Rev.* **2008**, *27*, 103–118.

(25) Kumar, C. C.; Nie, H.; Armstrong, L.; Zhang, R.; Vijay-Kumar, S.; Tsarbopoulos, A. *FEBS Lett.* **1998**, *429*, 239–248.

(26) Khalili, P.; Arakelian, A.; Chen, G.; Plunkett, M. L.; Beck, I.; Parry, G. C.; Doñate, F.; Shaw, D. E.; Mazar, A. P.; Rabbani, S. A. A non-RGD-based integrin binding peptide (ATN-161) blocks breast cancer growth and metastasis in vivo. *Mol. Cancer Ther.* **2006**, *5*, 2271–2280.